nature communications

Article

https://doi.org/10.1038/s41467-025-58093-x

The stomatin-like protein StlP organizes membrane microdomains to govern polar growth in filamentous actinobacteria under hyperosmotic stress

Received: 18 January 2024

Accepted: 7 March 2025

Published online: 18 March 2025

Check for updates

Xiaobo Zhong[1], Sarah S. M. Baur[2], Veronique M. A. Ongenae[1], Guillermo Guerrero Egido[1], Shraddha Shitut[1], Chao Du[1], Erik Vijgenboom[1], Gilles P. van Wezel[1], Victor Carrion Bravo[3], Ariane Briegel[1,4], Marc Bramkamp[2] & Dennis Claessen[1]

The cell wall represents an essential structure conserved among most bacteria, playing a crucial role in growth and development. While extensively studied model bacteria have provided insights into cell wall synthesis coordination, the mechanism governing polar growth in actinobacteria remains enigmatic. Here we identify the stomatin-like protein StlP as a pivotal factor for orchestrating polar growth in filamentous actinobacteria under hyperosmotic stress. StlP facilitates the establishment of a membrane microdomain with increased membrane fluidity, a process crucial for maintaining proper growth. The absence of StlP leads to branching of filaments, aberrant cell wall synthesis, thinning of the cell wall, and the extrusion of cell wall-deficient cells at hyphal tips. StlP interacts with key components of the apical glycan synthesis machinery, providing protection to filaments during apical growth. Introduction of StlP in actinobacteria lacking this protein enhances polar growth and resilience under hyperosmotic stress, accompanied by the formation of a membrane microdomain. Our findings imply that stomatin-like proteins, exemplified by StlP, confer a competitive advantage to actinobacteria encountering hyperosmotic stress. Given the widespread conservation of StlP in filamentous actinobacteria, our results propose that the mediation of polar growth through membrane microdomain formation is a conserved phenomenon in these bacteria.

The cell wall is considered an essential structure in bacteria that protects cells from environmental stresses[1,2]. To enable bacterial growth, the cell wall needs to be expanded, which involves inserting new cell wall material at the sites of growth. Elongation of rod-shaped cells typically occurs in two distinct manners[3]. Some rod-shaped bacteria, such as *Escherichia coli* and *Bacillus subtilis* elongate by incorporating new cell wall material in a rather diffuse manner in the cylindrical part of the cell[4]. By contrast, other bacteria grow by inserting new cell wall

[1]Molecular Biotechnology, Institute of Biology, Leiden University, Leiden, The Netherlands. [2]Institute for General Microbiology, Christian-Albrechts-University of Kiel, Kiel, Germany. [3]Departamento de Microbiología, Facultad de Ciencias, Campus Universitario de Teatinos s/n, Universidad de Málaga, 29010 Málaga, Spain. [4]Present address: Integrative Structural Cell Biology Unit, Department of Structural Biology and Chemistry, CNRS UMR 3528, Institut Pasteur, 75724 Paris, France. e-mail: d.claessen@biology.leidenuniv.nl

material at the cell poles, referred to as polar growth, which is widespread in actinobacteria[5,6]. This mode-of-growth has been well studied in actinomycetes, which are filamentous bacteria that form branched mycelial networks in soil environments. In their natural environment, actinomycetes are often confronted with suboptimal conditions, such as fluctuations in water availability causing dramatic osmotic imbalances[7]. Paradoxically, we recently showed how conditions of hyperosmotic stress causes shedding of the cell wall in several actinomycetes, implying that such conditions interfere with the process of cell wall growth[8].

Polar growth in actinomycetes is guided by the cytoskeletal protein DivIVA, which localizes in actively growing tips acting as a scaffold for other proteins involved in organizing tip growth, such as the coiled-coil protein Scy and the intermediate filament-like protein FilP[9–11]. Unlike Scy and FilP, DivIVA plays an essential function in polar growth, by directly interacting with the machinery involved in synthesis of peptidoglycan, a major constituent of the cell wall[12,13]. Both partial depletion and overproduction of DivIVA significantly altered cell shape and caused irregular branching[9]. Scy is an unusual long coiled-coil protein that co-localizes with DivIVA at hyphal tips. Scy was suggested to form higher order assemblies and thereby serves as a hub to stabilize the tip-organizing center, which also includes cell division proteins and proteins involved in chromosome segregation[11,14,15]. Collectively, these proteins facilitate that cell wall synthesis is coordinated with chromosome segregation to ensure proper growth and development of the mycelium.

DivIVA also interacts with the putative cellulose synthase CslA[16]. The glycan produced by CslA is thought to provide protection to the tips, which are constantly remodeled during growth, in particular under conditions of osmotic stress[16]. Synthesis of the cellulose-like glycan not only depends on the synthase CslA, but also on a range of other proteins that are all encoded in a conserved gene cluster (Supplementary Fig. 1A). Together with CslA, the radical copper oxidase GlxA are the key proteins responsible for synthesis and likely modification of the glycan[17,18]. Following synthesis of the glycan, the lytic polysaccharides monooxygenase LpmP and endoglucanase CslZ facilitate deposition of the glycan chain at the cell surface, possibly by creating a passage through the thick peptidoglycan (PG) layer[19]. The cooperation of CslA/GlxA and CslZ/LpmP implies that a multicomplex is established at the tip related to the proper synthesis and secretion of the cellulose-like glycan.

One of the proteins in the cellulose biosynthetic gene cluster that has not been studied encodes a stomatin/prohibitin/flotillin/HflK/C (SPFH)-domain protein, hereinafter referred to as StlP (for stomatin-like protein). The SPFH-superfamily proteins facilitate formation of lipid rafts, which in eukaryotes often contain protein complexes that collectively carry out important biological processes, such as ion channel regulation and touch sensation[20,21]. Notably, prokaryotic SPFH proteins, such as flotillins, also form comparable structures known as functional membrane microdomains (FMMs)[22,23]. These FMMs were shown to be involved in cell wall biosynthesis in *B. subtilis*[24] and *Staphylococcus aureus*[25]. Additionally, it was revealed that, in *B. subtilis*, flotillins play a direct role in controlling membrane fluidity homeostasis[26] with their expression intriguingly regulated by stress-specific signals[27].

In this study, we reveal the pivotal role of StlP in coordinating the creation of a microdomain crucial for sustaining tip growth in *Streptomyces coelicolor* during hyperosmotic stress conditions. The absence of StlP leads to anomalous hyphal shape alterations and, notably, the expulsion of cells lacking their cell wall. StlP undergoes polymerization into oligomers and localizes within the membrane, culminating in the formation of a membrane region characterized by heightened fluidity. This phenomenon is essential for harmonizing the growth of both membrane and cell wall during tip extension. Significantly, the ectopic expression of StlP in actinomycetes, known for naturally extruding wall-deficient cells, effectively prevents such extrusion. These findings collectively underscore the significance of StlP in establishing a membrane microdomain at hyphal tips, thereby playing a critical role in facilitating proper cell wall assembly under hyperosmotic stress conditions in filamentous actinobacteria.

Results

StlP is a stomatin-like protein in *Streptomyces coelicolor*

StlP is encoded in the conserved cellulose biosynthesis gene cluster in streptomycetes and located downstream of *lpmP*[19] (Supplementary Fig. 1A). Analysis of protein domains with InterPro and structure prediction via AlphaFold reveal that StlP contains three domains: a disordered region (aa 1-100), followed by a transmembrane hairpin composed by two helices (aa 106-126 and 149-168), and a SPFH (stomatin, prohibitin, flotillin, HflK/C) domain (aa 209-311) (Supplementary Fig. 1B, C).

Considering the diverse membrane topologies observed in members of the SPFH superfamily[28], we examined the membrane topology of StlP to determine its classification within the family of SPFH-containing proteins. In silico analyses predicted that the C-terminal SPFH domain of StlP is in the cytoplasm (Supplementary Fig. 1D). To validate this prediction, we employed a β-lactamase assay in which this enzyme was fused to the C-terminus of StlP as described[29]. *E. coli* cells expressing functional StlP-BlaM_{NS} fusions demonstrate sensitivity to ampicillin, in contrast to cells expressing BlaM_{FL} with its original signal peptide (Supplementary Fig. 1E–G). This result confirms that the C-terminal SPFH domain of StlP is situated in the cytoplasm, consistent with the observed membrane topology in podocin/stomatin family proteins[20] and its N-terminal transmembrane hairpin. In contrast to StlP, other SPFH-like proteins from *S. coelicolor* have a significantly different predicted membrane topology (Supplementary Fig. 2). A phylogenetic analysis, utilizing amino acid sequences from well-known prokaryotic and eukaryotic SPFH proteins, revealed that *S. coelicolor* StlP and Mouse stomatin STOML-1 form a monophyletic clade, indicating that StlP resembles a stomatin-like protein (Supplementary Fig. 3A). Further sequence alignment of StlP with other stomatins indicates that *Streptomyces* StlP contains the signature proline[30] residue required for membrane hairpin formation and a comparable domain arrangement (Supplementary Fig. 3B). This alignment suggests that StlP shares more similarities with eukaryotic stomatins than prokaryotic stomatins. Indeed, structural superposition shows that the stomatin domain (StlP_{SD}) of StlP aligns better with Mouse stomatin (MmStomatin) than the bacterial stomatin FliL (Supplementary Fig. 3C, D). In summary, these findings collectively establish StlP as a novel stomatin-like protein, containing a classic N-terminal transmembrane hairpin and stomatin domain, within the prokaryotic family of SPFH proteins.

StlP is important for morphogenesis under hyperosmotic stress conditions

To investigate the function of StlP, a *stlP* mutant (Δ*stlP*) was created that contained a Tn5062 transposon insertion, positioned upstream of the stomatin domain. This constructed *stlP* mutant was used to study its phenotype in various conditions. The *stlP* mutant displayed significantly reduced growth rates in both TSBS and LPB liquid medium, which contain 10 and 22% sucrose, respectively (Fig. 1A and Supplementary Fig. 4A). On MS agar medium (without sucrose), no apparent differences in growth were observed between the parent and the *stlP* mutant (Supplementary Fig. 4B). By contrast, when grown on LPMA agar medium (containing 22% sucrose), the average diameter of individual colonies of the *stlP* mutant (1.4 ± 0.3 mm) was significantly reduced compared to the wild-type strain (3.8 ± 0.6 mm) (Fig. 1B, C), suggesting that growth was severely hampered. Furthermore, we noticed that excess membrane was extruded from hyphal tips of the *stlP* mutant, as evident in the FM5-95 panels comparing M145 and Δ*stlP*

https://doi.org/10.1038/s41467-025-58093-x

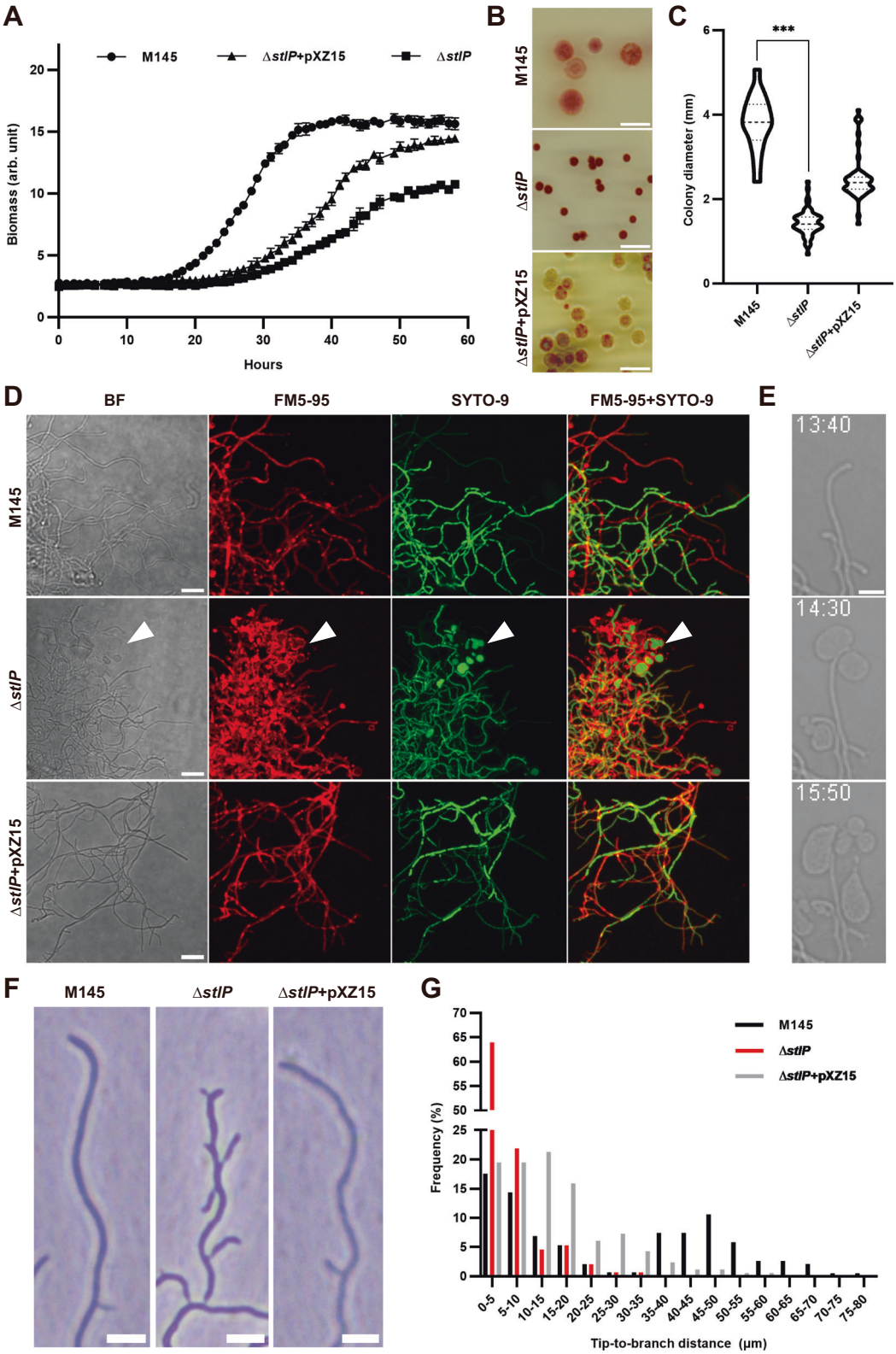

in Fig. 1C. Additionally, we observed many DNA-containing vesicles present in the medium (Fig. 1D) that were reminiscent of cell wall-deficient cells extruded by several filamentous actinobacteria. These vesicles were absent in the parental strain, consistent with earlier findings[8]. Time-lapse imaging revealed that the vesicles were extruded from hyphal tips (Fig. 1E and Supplementary Movies 2). Quantification revealed that the mutant formed 2.5×10^5 vesicles ml^{-1}, while none were found in the parental strain (Supplementary Fig. 5). Importantly, the significant reduced colony and formation of vesicles were also observed in the full-length *stlP* mutant ($\Delta stlP_{FL}$) generated via homologous recombination (Supplementary Fig. 6). To confirm that these phenotypes were caused by the absence of StlP, we introduced plasmid pXZ15 in the mutant, in which *stlP* is expressed from the constitutive *gapAp* promoter. Reintroduction of this plasmid partially restored the growth speed in liquid media (Fig. 1A and Supplementary Fig. 4A) and the average colony diameter on LPMA medium

Fig. 1 | The stomatin-like protein StlP is important for morphogenesis in *S. coelicolor*. **A** Growth of *S. coelicolor* M145, its *stlP* mutant and the complemented strain (Δ*stlP* + pXZ15) measured using a BioLector. Strains were grown in L-phase broth (LPB) medium, and biomass was measured in arbitrary units in triplicates. Error bars represent the standard error of the mean. **B** Colonies of *S. coelicolor* M145, the *stlP* mutant and the complemented strain (Δ*stlP* + pXZ15) after 5 days of growth. **C** Quantitative measurement of average colony diameters. The number was 17 for the wild-type strain (M145), 58 for the *stlP* mutant and 56 for the complemented mutant. ***$p < 0.001$; unpaired two-tailed Student's *t* test. **D** Mycelial morphology of the strains grown on solid L-phase medium agar (LPMA) medium. 16 h-old mycelium was labeled with SYTO-9 (stains nucleic acids; green) and FM5-95 (lipid stain; red). BF brightfield. Cell wall-deficient (CWD) cells are indicated with the white arrowhead. **E** Stills of Supplementary Movie 1 showing growth of the *stlP* mutant on LPMA medium. Micrographs were taken every 10 min. **F** The absence of StlP causes hyperbranching in *S. coelicolor*. Hyphae were imaged after 16 h of growth on cellophane membranes overlaying LPMA plates. Note that reintroduction of *stlP* expressed from the constitutive *gapAp* promoter (pXZ15) restores normal branching in the Δ*stlP* mutant. **G** Histograms showing the tip-to-branch distances in hyphae of M145, its *stlP* mutant and the complemented mutant (Δ*stlP* + pXZ15). Strains were grown for 16 h. The number of tip-to-branch distances was 188 for the wild-type strain (M145), 282 for the *stlP* mutant and 192 for the complemented mutant. Scale bars represent 5 mm (**B**), 50 μm (**D**) and 5 μm (**E**, **F**), respectively.

(2.5 ± 0.5 mm) (Fig. 1B, C), while extrusion of membranes and DNA-containing vesicles was also reduced by 80% (Fig. 1D and Supplementary Fig. 5).

Microscopy analysis also indicated that the hyphal branching pattern was affected by the deletion of *stlP* (Fig. 1F, Supplementary Fig. 4D and Supplementary Movies 1 and 2). More specifically, the number of branches was dramatically increased in the *stlP* mutant when grown under hyperosmotic stress conditions (LPMA medium) (Fig. 1F). A similar effect was observed when the sucrose in LPMA (0.64 M) was replaced with NaCl (0.32 M, Supplementary Fig. 7). To quantitatively compare branching between the strains, we measured the distance from the tip to the proximal branching point in hyphae (Supplementary Figs. 4D and 7). Deletion of *stlP* changed the distribution of the tip-to-branch distances significantly. We found that more than 60% of all hyphae in Δ*stlP* had a proximal branch within the first 5 μm from the tip (Fig. 1G), as compared to approximately 15% for the parent and the complemented mutant. Also, no hyphae of the *stlP* mutant branched further than 35 μm from the tip. Additionally, when grown on MS medium, hyphae with a tip-to-branch distance less than 10 μm accounted for 3.6% and 8.9% of the parent and mutant strain, respectively (Supplementary Fig. 4E). This suggests a mild impact on the branching pattern due to the deletion of *stlP* under normal growth conditions. Taken together, these findings underscore that the absence of StlP significantly affects polar growth and causing an increase in the emergence of lateral branches in *S. coelicolor*, particularly manifesting under conditions of hyperosmotic stress.

StlP is important for spatially confining cell wall synthesis to hyphal tips

To investigate the localization of StlP, we introduced pXZ16 into *S. coelicolor* M145, thereby constitutively expressing a C-terminal mCherry fusion to StlP. Foci of StlP-mCherry mostly localized at growing tips and emerging branches (Fig. 2A). We also localized the polar growth determinant DivIVA in the presence and absence of StlP by expressing a DivIVA-mCherry fusion from the constitutive *gapAp* promoter. Interestingly, in the absence of StlP, DivIVA-mCherry was not only localized to hyphal tips but was also found in numerous foci along the cylindrical part of the filaments (Fig. 2B), suggesting diffusion of cell wall synthesis from the apex. In agreement, nascent PG was incorporated at multiple sites along the filament in the *stlP* mutant (Fig. 2C), coinciding with an increase in the average diameter of the hyphae (Fig. 2D). Using calcofluor white staining, we observed that multiple synthesis foci of the cellulose-like glycan produced by CslA appeared at both established and emerging hyphal tips in the *stlP* mutant, in contrast to the parental strain (Fig. 2E). Furthermore, quantitative analysis revealed a significant decrease (approximately 65%) in the accumulated glycan at the hyphal tips of the *stlP* mutant. Consistent with other mutants affected in apical glycan synthesis[19], we indeed noticed that the reduced glycan levels made the *stlP* mutant sensitive to lysozyme (Fig. 2G). Glycan deposition and lysozyme resistance were restored when the complementation plasmid pXZ15 was introduced in the *stlP* mutant (Fig. 2E–G).

To accurately evaluate the effect of the absence StlP on cell wall thickness of *S. coelicolor*, we conducted a thorough examination by preparing and imaging sacculi of M145 and the Δ*stlP* strains using cryo-electron tomography (cryo-ET). The analysis of cell wall thickness measurement revealed a significant reduction in the overall cell wall thickness upon *stlP* deletion compared to the parental strain. Specifically, the thickness in the apical region decreased from 35.5 ± 1.7 nm to 6.4 ± 0.6 nm, while the thickness in the subapical region was reduced from 37.1 ± 2.3 nm to 9.9 ± 0.6 nm (Fig. 2H, I and Supplementary Movies 3 and 4). These results demonstrate the importance of StlP for cell wall synthesis and thickness of *S. coelicolor*.

To establish how StlP contributes to delocalized cell wall synthesis, we tested interactions of StlP with the proteins involved in tip growth and cellulose biosynthesis. To this end, constructs were generated that produced C-terminal fusions of StlP, LpmP, SCO2835, CslA, GlxA, CslZ, DivIVA, Scy and FilP to either the T25 or T18 fragments of the adenylate cyclase, respectively. Co-transformation of these constructs in *E. coli* BTH101 revealed that StlP did not interact with DivIVA, Scy or FilP. However, StlP robustly interacts with LpmP, SCO2835, CslA and CslZ, but also with itself and weakly interacts with GlxA (Supplementary Fig. 8A, B). Pull-down experiments using *E. coli* BL21 cells expressing a C-terminal 8×His-tagged StlP (StlP-8His), a C-terminal Flag-tagged CslA (CslA-Flag), and GlxA confirmed that StlP-8His effectively pulled down CslA-Flag and GlxA, as demonstrated by size exclusion chromatography and immunoblotting analyses (Supplementary Fig. 8D, E). Additionally, Native-PAGE analysis revealed the presence of the StlP-8His/CslA-Flag/GlxA complex with an approximate molecular weight of 480 kDa (Supplementary Fig. 8F). To validate these findings, we investigated the interactions between StlP, CslA, and GlxA in *Streptomyces*, and performed bimolecular fluorescence complementation (BiFC) experiments. To this end, eGFP was split into two fragments, $eGFP_N$ and $eGFP_C$, which were fused to either the N- or C-terminus of StlP, CslA, or GlxA. For GlxA, the $eGFP_C$ fragment was specifically inserted between its signal peptide and its N-terminal transmembrane anchor, ensuring that the eGFP signal remained localized to the inner membrane following GlxA secretion. Constructs were generated using apramycin-resistant pSET152 and thiostrepton-resistant pWHM3-oriT backbones, with expression driven by the constitutive *gapAp* promoter. Various constructs pairs were conjugated into the wild-type strain M145, and protein interactions were assessed based on detectable eGFP fluorescence at hyphal tips, resulting from the reconstitution of eGFP fragments ($eGFP_N$ and $eGFP_C$) through complementation. Controls included strains expressing individual protein fusions. Results showed that $eGFP_N$ fused to the C-terminus of StlP complemented $eGFP_C$ fragments fused to either the N- or C-terminus of CslA, indicating robust StlP-CslA interactions (Fig. 3A and Supplementary Fig. 9). No fluorescence was observed between StlP and GlxA constructs (Fig. 3B and Supplementary Fig. 9). $eGFP_C$ fused to the N-terminus of GlxA complemented $eGFP_N$ fused to the C-terminus of CslA, demonstrating a strong interaction between

https://doi.org/10.1038/s41467-025-58093-x

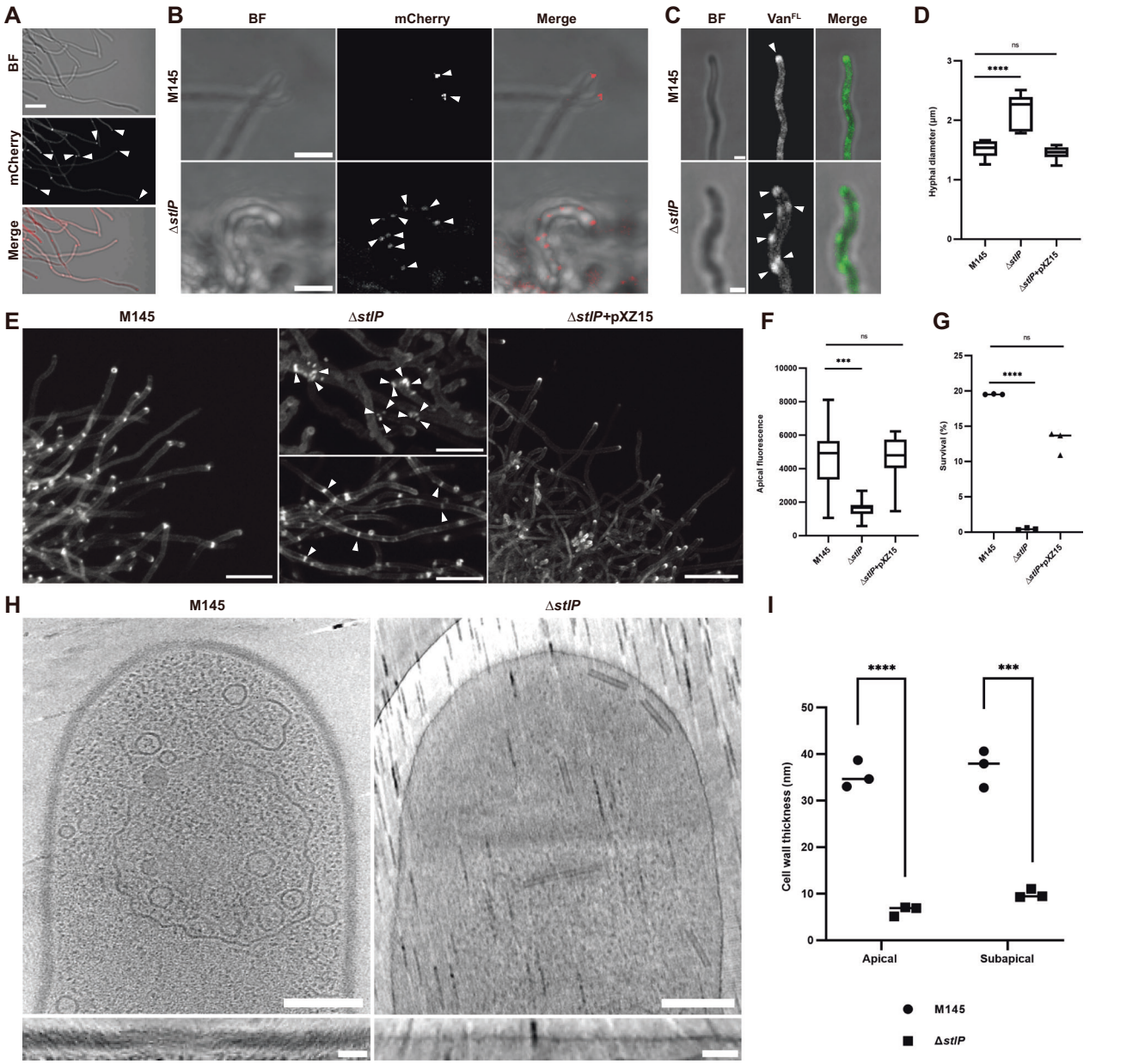

CslA and GlxA (Fig. 3 and Supplementary Fig. 9). These findings establish that StlP directly interacts with components of the cellulose biosynthesis complex and spatially confines cell wall synthesis to hyphal tips in *S. coelicolor*.

StlP oligomerizes and forms membrane microdomain at hyphal tips of *S. coelicolor*

Bacterial two-hybrid analysis suggested that StlP interacts with itself but also with components of the machinery involved in glycan synthesis (Supplementary Fig. 8A). To test if StlP interacts with itself via the stomatin domains, the corresponding domain (aa 204-326; referred to as $StlP_{SD}$) was expressed in *E. coli* BL21(DE3). The $StlP_{SD}$ monomer was expressed, showing a predicted molecular mass of 19.6 kDa (Fig. 4A). When 20 μg of concentrated $StlP_{SD}$ protein (1 mg ml^{-1}) were loaded in a SDS-PAGE gel, a ladder of oligomers was found, suggesting that monomers readily self-assemble and are resistant to SDS (Fig. 4A). Notably, analysis of 20 μg of concentrated $StlP_{SD}$ protein using Native-PAGE revealed a predominance of heptamers, along with smaller amounts of decamers and trimers (Fig. 4A). To obtain more insight into self-assembly of StlP, we predicted the partial structure of StlP (aa 106-326), encompassing the two N-terminal TMHs (aa 106-126 and aa 149-168) and the stomatin domain (aa 209-311) using AlphaFold 2.0. When six StlP monomers were used as input, an ordered hexamer and partial ring-like structure was obtained, while ten monomers assembled into a symmetric ring (Fig. 4B and Supplementary Fig. 10). These results suggest that StlP can assemble into oligomers via its stomatin domain at high concentrations, which in the full-length protein would probably result in formation of a membrane microdomain via its two N-terminal transmembrane helices.

In bacteria, SPFH proteins are involved in membrane fluidity homeostasis, evidenced by FloT and FloA that fluidize the membrane and absence of them leads to an overall rigidification[24,26]. We therefore predicted that the oligomerization of StlP leads to the formation of a local membrane region with increased fluidity (RIF) at hyphal tips. To test this, we stained mycelia of *S. coelicolor* with $DilC_{12}$, a lipid dye with high specificity for fluid membranes due to its short hydrocarbon tail[31,32]. We observed bright $DilC_{12}$ staining RIFs at hyphal tips, and also along hyphae grown for 16 h in LPB medium (Fig. 4C). The signal corresponding to $DilC_{12}$ staining was absent from hyphal tips of the *stlP* mutant and restored in the complemented strain (Fig. 4C). These

Fig. 2 | StlP localizes to hyphal tips and affects cell wall synthesis. A Localization of StlP-mCherry (red) in the wild-type strain carrying plasmid pXZ16. White arrowheads indicate the location of StlP-mCherry at hyphal tips (bright spots). BF brightfield. **B** Localization of DivIVA-mCherry (red) in the wild-type strain and the *stlP* mutant, both of which carry plasmid pXZ17. Strains were grown in L-phase broth (LPB) medium for 16 h prior to imaging. The arrowheads indicate the location of DivIVA-mCherry (bright spots). BF brightfield. **C** Visualization of nascent peptidoglycan in *S. coelicolor* strains using fluorescent vancomycin (Van^{FL}; green) staining. White arrows indicate peptidoglycan (PG) synthesis sites (bright spots). BF brightfield. **D** Deletion of *stlP* increases hyphal diameter. Quantification was done by measuring the hyphal diameter after staining with FM5-95. Box plots display the distribution of hyphal diameter measurements. The center line represents the median (50th percentile). The box spans from the first quartile (25th percentile) to the third quartile (75th percentile), representing the interquartile range (IQR). Whiskers extend to the smallest and largest values within 1.5 times the IQR. Data points beyond this range are considered outliers and are shown as individual dots. $^{***}p < 0.001$; ns, not significant ($p = 0.37$); unpaired two-tailed Student's *t* test without corrections. **E** The absence of StlP affects proper deposition of the cellulose-like glycan. Foci are either splitting at hyphal tips (bright spots) or diffused (bright spots indicated by white arrowheads) along the filament in the *stlP* mutant. Strains were grown in LPB medium and fluorescent images were taken after 16 h of growth. Bars represent 20 µm. **F** Quantification of the cellulose-like glycan at hyphal tips using calcofluor white staining. For each tip, the total fluorescence in a square (1.5 µm by 1.5 µm) at the hyphal tip was measured using ImageJ software. For each strain, fluorescence at 10 tips was measured, and a square (1.5 µm by 1.5 µm) without fluorescence near the hyphal tip was used as the blank. Box plots display the distribution of apical fluorescence measurements. The center line represents the median (50th percentile). The box spans from the first quartile (25th percentile) to the third quartile (75th percentile), representing the interquartile range (IQR). Whiskers extend to the smallest and largest values within 1.5 times the IQR. Data points beyond this range are considered outliers and are shown as individual dots. $^{***}p < 0.001$; ns, not significant ($p = 0.91$); unpaired two-tailed Student's *t* test. **G** The absence of the cellulose-like glycan at hyphal tips increases lysozyme sensitivity of the *stlP* mutant. For each strain, ~1000 spores were plated on nutrient agar plates, and colony numbers were counted after 3 days. The percentage (number of colonies from plates with 0.25 mg ml^{-1} lysozyme divided by the number of colonies from plates without lysozyme) was used to evaluate the sensitivity of strains for lysozyme. Colony counts for plates with lysozyme were: wild-type strain (M145), 160/161/160; *stlP* mutant, 3/5/3; complemented mutant, 145/142/113. Colony counts for plates without lysozyme were: wild-type strain (M145), 929/822/708; *stlP* mutant, 861/814/773; complemented mutant, 935/1003/1179. *n* = three biological replicates; $^{****}p < 0.0001$; ns, not significant ($p = 0.10$); Mann–Whitney test. Error bars represent the standard error of the mean. **H** Stills from Supplementary Movie 3 and 4 show cryo-ET images of sacculi from the wild-type (top left panel) and the *stlP* mutant strain (top right panel). The bottom panel depicted the corresponding straightened cell wall at the apical region of each strain. **I** Cell wall thickness measurements of the wild-type and *stlP* mutant strain. Our observation here could not be statistically analyzed due to generating large dataset from Cryo-ET is challenging. *n* = three technical replicates; $^{****}p < 0.0001$; $^{***}p < 0.001$; unpaired two-tailed Student's *t* test. Error bars represent the standard error of the mean. Bars represent 20 µm (**A**), 5 µm (**B**), 1 µm (**C**), 10 µm (**E**), 200 nm (**H**, top panel), and 50 nm (**H**, bottom panel), respectively.

results suggest that hyphal tips possess a RIF, which is dependent on the presence of StlP. To substantiate the presence of RIFs at hyphal tips, we conducted a quantitative assessment of membrane fluidity using the membrane-intercalating dye Laurdan. This dye exhibits a shift in fluorescence emission wavelength based on membrane fluidity[31,33]. After culturing mycelia of M145 and its *stlP* mutant in LPB medium for 16 h, we stained them with Laurdan and then calculated the general polarization (GP) value at the tip region of each hypha (see "Materials and methods"). In the absence of *stlP*, the average GP value (−0.09 ± 0.08) increased compared to its parental strain (−0.12 ± 0.13), inferring a decreased membrane fluidity in the *stlP* mutant (Fig. 4D, E). Furthermore, the apical membrane fluidity of the *stlP* mutant could be restored by raising the growth temperature to 37 °C (Fig. 4F), which aligns with the idea that elevated temperatures contribute to membrane phase transitions, leading to an increased fluidity[34]. Altogether, these results reveal that StlP oligomerizes and forms membrane domains with enhanced membrane fluidity at hyphal tips of *S. coelicolor*.

Morphogenesis controlled by StlP is conserved in filamentous actinobacteria

Our results indicate that StlP contributes to proper cell wall synthesis and membrane organization under hyperosmotic stress, and thereby controls morphogenesis of *S. coelicolor*. To see how prevalent StlP is, we combined PSI-BLAST and TMHMM prediction to identify stomatin homologs of StlP in the dataset of 15045 RefSeq representative bacteria and archaea. This analysis showed that the majority of StlP homologs are present in actinobacteria, while a few are also present in *Rhizobium* (Fig. 5). Furthermore, inside the filamentous actinobacteria, StlP orthologs are present in genera including *Streptomyces, Kitasatospora* and *Streptacidiphillus* (Fig. 5). In some clades of these bacteria, all members have an orthologue of StlP, while in others StlP is less common or virtually absent. Notably, *Kitasatospora viridifaciens* DSM40239 is among the clades that lack StlP (Fig. 5).

To see how widespread the function of StlP is in other actinobacteria, the construct pXZ15, wherein the *stlP* was expressed from the constitutive *gapAp* promoter, was introduced into *Kitasatospora viridifaciens* DSM40239 via conjugation, which is known to extrude wall-deficient cells under hyperosmotic stress[8,35]. Importantly, constitutive expression of *stlP* induced the formation of a fluid membrane microdomain at hyphal tips in *K. viridifaciens*, as evidenced by $DilC_{12}$ staining (Fig. 6A). Furthermore, constitutive expression of *stlP* significantly increased the average membrane fluidity of hyphae (Fig. 6B, C) and allowed colonies to cope much better with hyperosmotic stress, as shown by the strongly increased colony diameter of the strain expressing *stlP* (2.75 ± 0.6 mm) as compared to the parental strain (1.25 ± 0.9 mm) (Fig. 6D, E) and by the reduced lateral branching of *K. viridifaciens* (Fig. 6F, G). Furthermore, constitutive expression of *stlP* largely abolished the extrusion of wall-deficient cells in *K. viridifaciens* (Fig. 6H, I). This response to induced StlP expression was specific, as the constitutive expression of the endogenous HflK/C protein, encoded by *BOQ63_030050* and sharing 21% sequence identity with StlP, was unable to prevent the extrusion of cell wall-deficient cells in *K. viridifaciens* (Supplementary Figs. 11 and 12). Taken together, these results demonstrate that the stomatin-like protein StlP controls growth of filamentous actinobacteria under hyperosmotic stress by the localized control of membrane fluidity, and this phenomenon is well-conserved in filamentous actinobacteria.

Discussion

Stomatin-like proteins are ubiquitous in all domains of life. A universal feature of these proteins is to form functional nanoscale microdomains in biological membranes. In turn, these microdomains serve as platforms to locate protein complexes involved in important biological processes, such as transducing mechanosensory signals in mice and modulation of ion channels in mammalian cells[36–38]. The recent structural analysis of the stomatin-like protein FliL from *Vibrio alginolyticus* showed that FliL shares some structural elements with eukaryotic stomatins, suggesting that stomatin-like proteins are conserved from mammals to bacteria[38]. Here, we identified the stomatin-like protein StlP as a novel polar growth determinant in filamentous actinobacteria.

Establishing cell polarity and ensuring robust polar growth are important for actinobacteria to cope with environmental fluctuations. Our work shows that the presence of a microdomain, coordinated by the stomatin-like protein StlP, contributes to survival in conditions of hyperosmotic stress. The presence of this domain ensures that the synthesis of cell wall components remains localized at hyphal tips,

https://doi.org/10.1038/s41467-025-58093-x

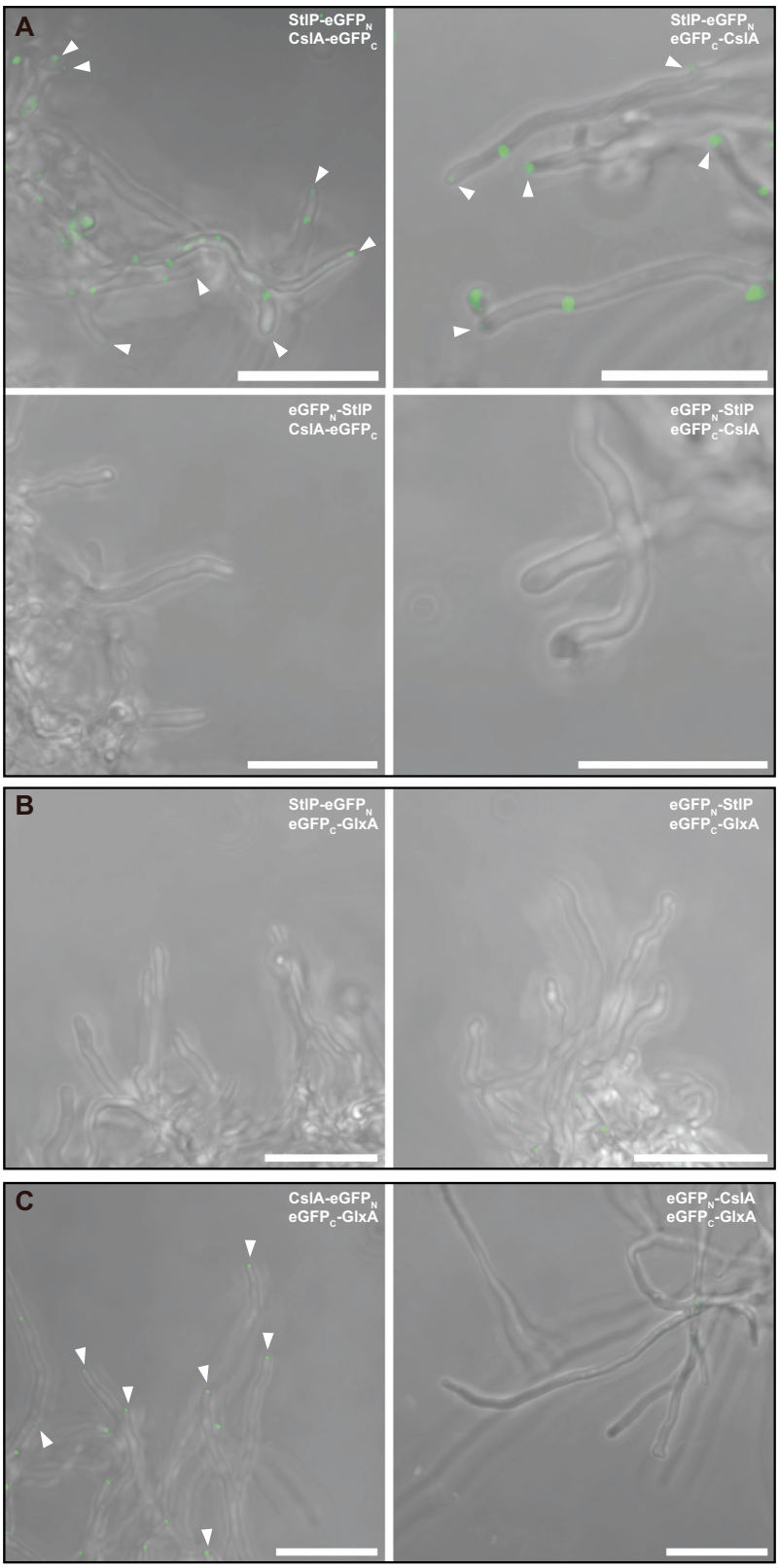

Fig. 3 | BiFC analysis of StlP, CslA, and GlxA interactions in *Streptomyces*. Detection of interactions between the stomatin-like protein (StlP) and the cellulose synthase-like protein (CslA) (**A**), StlP and the galactose oxidase-like protein (GlxA) (**B**), and CslA and GlxA (**C**) using bimolecular fluorescence complementation (BiFC). The wild-type *Streptomyces coelicolor* M145 strain was transformed with plasmids expressing the indicated protein fusion pairs. Control experiments with M145 strain expressing individual protein fusion are presented in Supplementary Fig. 9. White arrows indicate the appearance of enhanced-green fluorescent protein (eGFP) fluorescence at hyphal tips demonstrating interactions between respective protein pairs. Bars represent 10 µm for all images.

https://doi.org/10.1038/s41467-025-58093-x

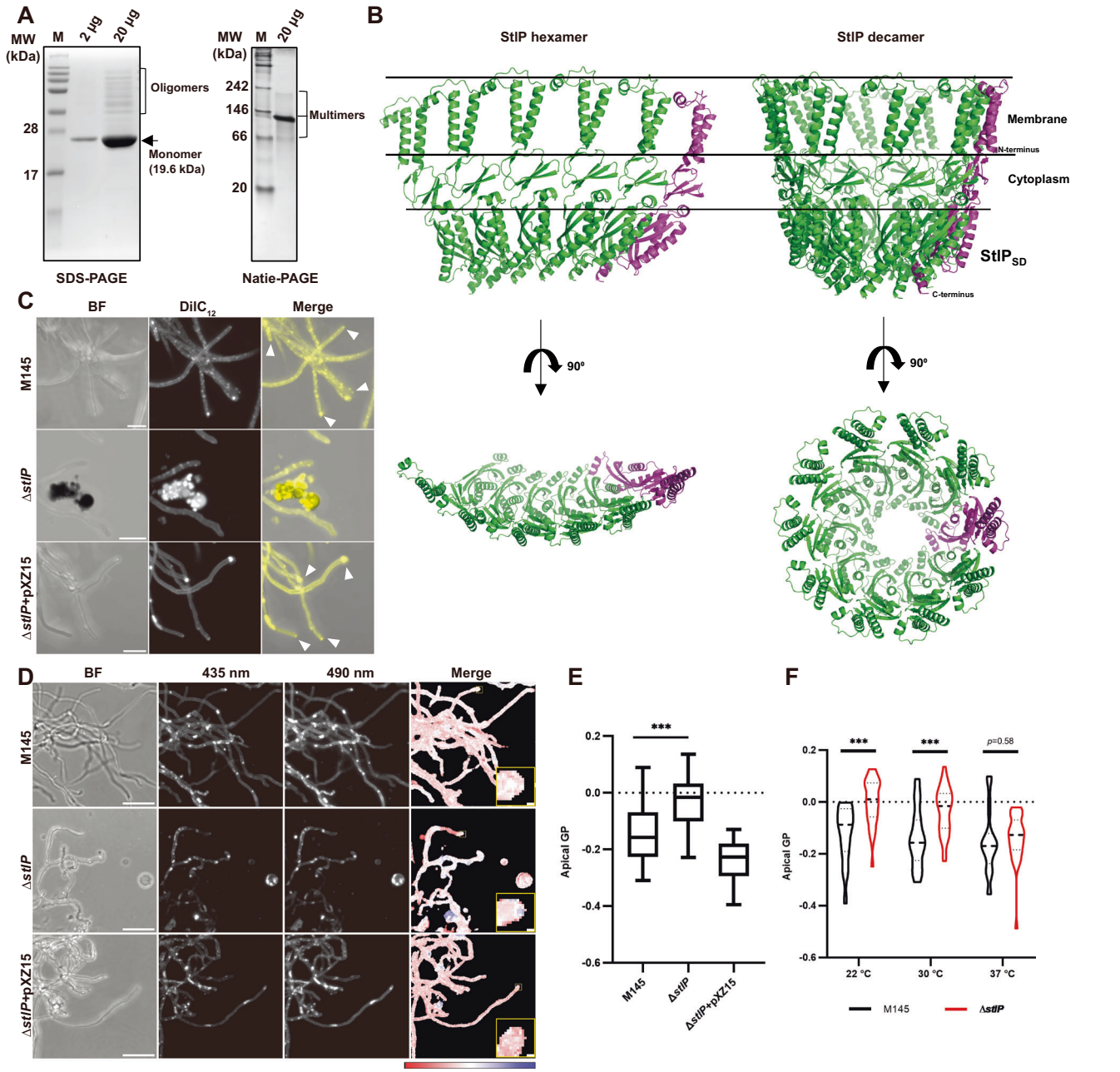

Fig. 4 | StlP oligomerizes and controls membrane fluidity at hyphal tips. A StlP assembles into oligomers, consistent with other stomatin proteins. The stomatin domain of StlP (StlP$_{SD}$) was purified and concentrated to 1 mg ml^{-1}. For the SDS-PAGE analysis, 2 and 20 µg StlP$_{SD}$ were loaded. For the Native-PAGE gel, 20 µg StlP$_{SD}$ was used. Protein bands were visualized with Coomassie blue staining. **B** AlphaFold predictions of an StlP hexamer (left) or decamer (right). The StlP decamer assembles into a 10-fold symmetric ring structure. For the prediction, the amino acid sequence spanning the two N-terminal transmembrane helices (TMHs) at positions 106-126 and 149-168, as well as the stomatin domain at positions 209-311 of StlP were used. Magenta represents an StlP monomer. Deletion of *stlP* increases membrane fluidity at hyphal tips of *S. coelicolor*. **C** Visualization of a fluid membrane region (yellow spots) at hyphal tips. 16 h-old cultures of *S. coelicolor* M145, the *stlP* mutant and the complemented mutant strain (Δ*stlP* + pXZ15) were incubated with 100 µM DiIC$_{12}$ and grown for a further 3 h in L-phase broth (LPB) liquid medium prior to imaging. White arrows indicate fluid regions at hyphal tips. Please note that the extruded cell wall-deficient (CWD) cells are highly fluid. BF brightfield. Qualitative (**D**) and quantitative (**E**) analysis of membrane fluidity using Laurdan staining. Mycelia from 16 h-old cultures of different strains were collected and labeled with 1 mM Laurdan. Red and blue pixels represent high and low fluidity, respectively (**D**). BF brightfield (**D**). The values in the graph (**E**) indicate the generalized polarization (GP), which ranges from −1 (more fluid) to +1 (less fluid). The number of measured tips was 27 for the wild-type strain (M145), 30 for the *stlP* mutant and 26 for the complemented mutant. Box plots display the distribution of apical fluorescence measurements. The center line represents the median (50th percentile). The box spans from the first quartile (25th percentile) to the third quartile (75th percentile), representing the interquartile range (IQR). Whiskers extend to the smallest and largest values within 1.5 times the IQR. Data points beyond this range are considered outliers and are shown as individual dots. ***$p < 0.001$; unpaired two-tailed Student's *t* test. **F** Increased growth temperature restores membrane fluidity of the *stlP* mutant. Here, strains were grown in LPB liquid medium at 22, 30 or 37 °C for 16 h and the membrane fluidity is indicated as GP value. Approximately 45 tips were measured for each strain. ***$p < 0.001$ for 22 °C and 30 °C; $p = 0.58$ for 37 °C; unpaired two-tailed Student's *t* test. Scale bar represents 5 µm (**C**), 10 µm (**D**, main images) and 0.5 µm (**D**, insets), respectively.

https://doi.org/10.1038/s41467-025-58093-x

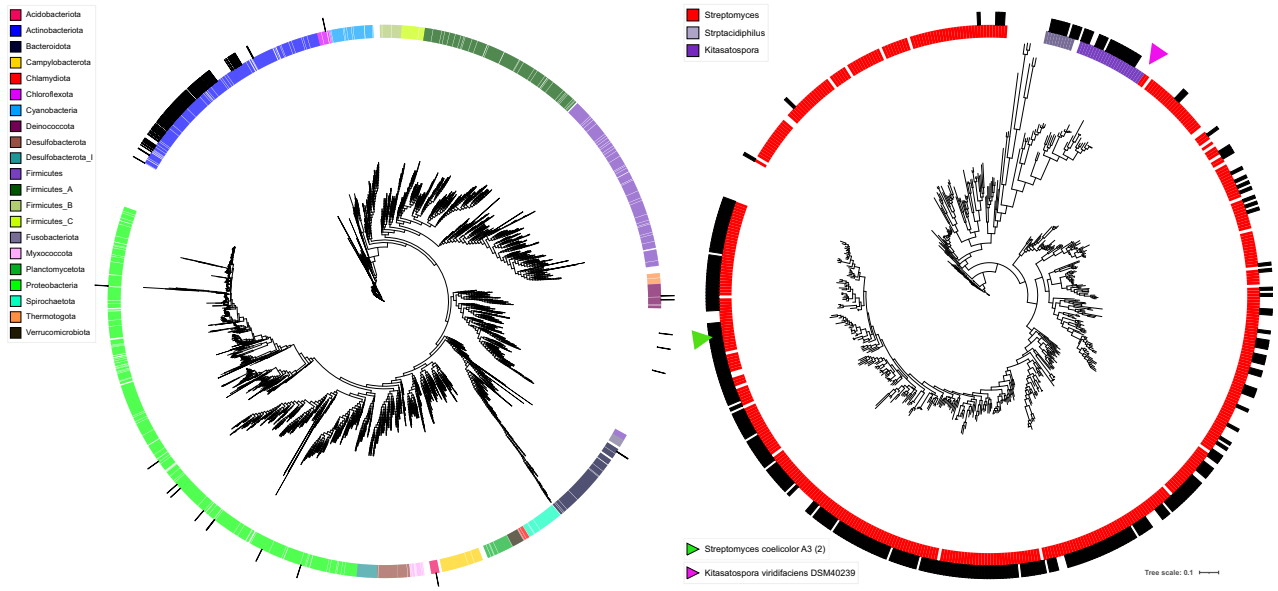

Fig. 5 | Phylogenetic analysis of the distribution of StlP proteins in Proteobacteria. Maximum-likelihood was used to construct the phylogenetic trees. Position-Specific Iterative (PSI)-BLAST and TransMembrane Hidden Markov Model (TMHMM) prediction were used to identify StlP homologs in the dataset of 15,405 reference sequence database (RefSeq) representative bacteria and archaea (left panel). The right panel indicates the distribution of StlP homologs in the genus of actinobacteria. The inner strips indicate different phyla (left panel) or genera (right panel), represented by different colors, while the outside black strip indicates StlP homologs. The green and pink arrowheads represent *Streptomyces coelicolor* A3(2) and *Kitasatospora viridifaciens* DSM40239, respectively.

which is pivotal for radial expansion of the colony. Indeed, the deletion of *stlP* leads to reduced expansion of the colony, coinciding with the formation of numerous small branches. We believe that this altered branching pattern has no direct benefit: escape from this stress, by radial growth, is hampered. However, under these conditions we see that hyphae also extrude wall-deficient cells, presumably due to the imbalance between membrane and cell wall synthesis. The formation of such cells may offer an alternative dispersal advantage for survival under hyperosmotic stress for other filamentous actinobacteria that lack StlP.

Stomatins oligomerize in cell membranes through interactions between their stomatin-domains, thus providing a scaffold for numerous other proteins. This functionality has been demonstrated for several stomatins, including mouse stomatin[37], *Pyrococcus horikoshii* stomatin[39] and the stomatin FliL of *Vibrio alginolyticus*[38]. Cross-linking studies and structure predictions demonstrate that the stomatin domain of StlP oligomerizes and that StlP interacts with the machinery involved in synthesis of a cellulose-like glycan. One of these proteins is the cellulose synthase-like protein CslA, which in turn directly interacts with DivIVA[16]. Interestingly, PG synthesis of actinomycetes is directed at hyphal tips in a DivIVA-dependent manner. More specifically, DivIVA recruits penicillin-binding proteins (PBPs) during polarized growth, as deduced from the detected interaction between DivIVA and PBP3 in *M. tuberculosis*[11,12]. StlP seems to contribute to establishing a localized region in the cellular membrane carrying crucial components of the so-called tip organizing center, which controls cell wall synthesis during the polar growth in filamentous actinobacteria (Fig. 7). Indeed, the observation of diffused PG and surface cellulose synthesis foci and dramatically reduced cell wall thickness of the *stlP* mutant indicated that PG synthesis is significantly weakened upon the deletion of *stlP* (Fig. 2). We thus propose a model for the cell wall synthetic machinery at hyphal tips when filamentous actinobacteria grow in hyperosmotic stress conditions. In this model, DivIVA guides the machinery responsible for peptidoglycan (PG) and surface cellulose-like glycan synthesis to the poles through interactions with CslA and PBPs. At these poles, the systems are restricted by the formation of StlP rings, which, in turn, induce localized membrane fluidization (Fig. 7). Here, the StlP ring enables these filamentous actinobacteria to produce robust cell walls during polarized growth under conditions of hyperosmotic stress. Without StlP, the membrane fluidity in the tip region decreases. Combined with the loss of localized cell wall synthesis, this leads to the extrusion of wall-deficient cells. Reversely, constitutive expression of StlP in species that naturally lack this protein prevents the typical extrusion of wall-deficient cells. Taken together, this work provides a plausible mechanism how wall-deficient cells are extruded in polar-growing actinobacteria. By interrupting cell wall synthesis, by exposing the cells to hyperosmotic stress or antibiotics, the coordinated balance between membrane and cell wall synthesis is lost. In turn, this leads to shedding of excess membranes from the polar growth sites and is facilitated by the localized weakening of the cell wall.

In summary, our work for the first time characterizes a stomatin-like protein that regulates tip growth in conditions of hyperosmotic stress. The strong phenotype associated with its absence make this also an interesting candidate to target in pathogenic bacteria that grow from the cell poles. In this context, it is noteworthy that mycobacteria have the ability to adopt a wall-deficient lifestyle[40], and it's worth highlighting that *Mycobacterium tuberculosis* possesses a StlP homolog.

Our study also advances the understanding of the functional divergence of the SPFH protein family, emphasizing their evolutionary specialization across taxa. Although conserved in both prokaryotes and eukaryotes, SPFH proteins have adapted to distinct roles. For example, while the stomatin-like protein StoA in filamentous fungi affects hyphal morphology without being essential for apical membrane microdomain formation[41], StlP in *Streptomyces* is critical for microdomain formation at hyphal tips. Interestingly, in bacteria, SPFH proteins appear to universally contribute to membrane fluidity and cell wall biosynthesis, with examples such as flotillin in *Bacillus subtilis*, which regulates MreB dynamics[24], and in *Staphylococcus aureus*, where it tethers PBP2a to facilitate peptidoglycan assembly[25]. Our findings reveal that StlP in *Streptomyces* not only regulates localized membrane fluidity but also impacts cellulose-like glycan biosynthesis, a key cell wall component. These observations suggest that SPFH proteins

https://doi.org/10.1038/s41467-025-58093-x

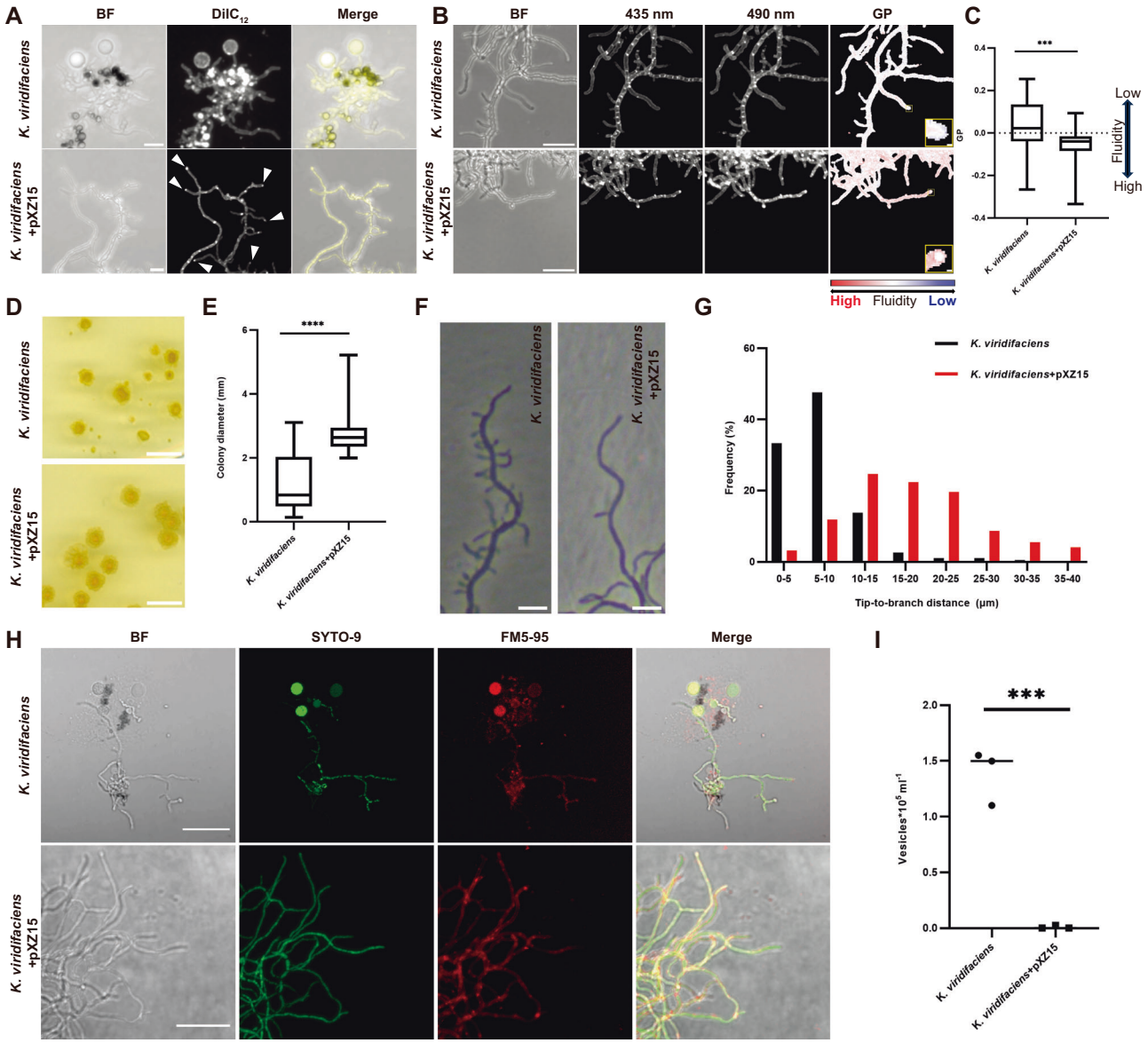

Fig. 6 | Enhanced robustness of *K. viridifaciens* growth under hyperosmotic stress conditions through constitutive StlP expression. A Visualization of fluid membrane regions at hyphal tips of a *K. viridifaciens* derivative constitutively expressing StlP (*K. viridifaciens* + pXZ15) compared to the parental wild-type. Images were obtained after $DiIC_{12}$ staining (yellow) of 16 h-old cultures followed by growth for 3 h in LPB liquid medium. White arrows indicate fluid regions (bright spots) at hyphal tips. BF brightfield. **B**, **C** Quantitively analysis of membrane fluidity using Laurdan staining. Mycelia from 16 h-old cultures were collected and labeled with 1 mM Laurdan (**B**). BF brightfield. The values in the graph (**C**) indicate the generalized polarization (GP), which ranges from −1 (more fluid) to +1 (less fluid). Red and blue pixels represent high and low fluidity, respectively. The number of tips measured was 37 (*K. viridifaciens*) and 45 (*K. viridifaciens* + pXZ15). Box plots display the distribution of apical fluorescence measurements. The center line represents the median (50th percentile). The box spans from the first quartile (25th percentile) to the third quartile (75th percentile), representing the interquartile range (IQR). Whiskers extend to the smallest and largest values within 1.5 times the IQR. Data points beyond this range are considered outliers and are shown as individual dots. ***$p < 0.001$; unpaired two-tailed Student's *t* test. **D** Constitutive expression of *stlP* from the *gapAp* promoter increases the average colony size of *K. viridifaciens*. Colonies of the wild-type strain and a derivative constitutively expressing StlP (*K. viridifaciens* + pXZ15) are shown after 7 days of growth. **E** Quantitative assessment of the average colony diameter ($n = 88$ for *K. viridifaciens* and $n = 84$ for *K. viridifaciens* + pXZ15). Box plots display the distribution of colony diameter measurements. The center line represents the median (50th percentile). The box spans from the first quartile (25th percentile) to the third quartile (75th percentile), representing the interquartile range (IQR). Whiskers extend to the smallest and largest values within 1.5 times the IQR. Data points beyond this range are considered outliers and are shown as individual dots. ****$p < 0.0001$; unpaired two-tailed Student's *t* test. **F** Constitutive expression of *stlP* from the *gapAp* promoter prevents hyperbranching. Individual hyphae were imaged after 16 h of growth on cellophane membranes overlaying solid L-phase medium agar (LPMA) plates. **G** Histograms indicating the distribution of tip-to-branch distances of *K. viridifaciens* with or without pXZ15. The number of filaments measured for each strain were 219 (*K. viridifaciens*) and 189 (*K. viridifaciens* + pXZ15). **H** Constitutive expression of StlP (from plasmid pXZ15) blocks the extrusion of wall-deficient cells in *K. viridifaciens*. 16 h-old mycelium was labeled with SYTO-9 (stains nucleic acids; green) and FM5-95 (lipid stain; red). BF, brightfield. **I** Quantification of cell wall-deficient cells was assessed after growing strains in LPB medium for 40 h (n = three biological replicates). Scale bars represent 5 µm (**A**, **F**), 10 µm (**B**, main images), 0.5 µm (**B**, insets), 5 mm (**D**) and 20 µm (**H**), respectively.

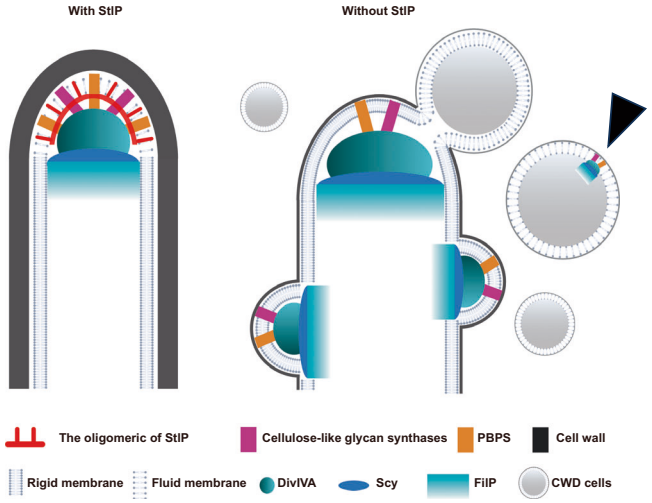

Fig. 7 | Proposed model for tip growth under conditions of hyperosmotic stress. StlP, a stomatin-like protein, undergoes oligomerization, creating an assembly on the membrane that facilitates the formation of microdomains. These microdomains induce local membrane fluidization and serve as a platform for coordinated cell wall synthesis, ensuring normal polar growth. In the absence of StlP (right panel), membrane fluidity diminishes in the tip region, coinciding with the diffusion of apical cellulose-like glycan and peptidoglycan synthesis foci, resulting in the loss of spatially confined cell wall synthesis. This weakens the cell wall, leading to the extrusion of cells with deficient walls. The black arrowhead points to a CWD cell that rebuilds its cell wall. Model created in BioRender. Claessen (2025) https://BioRender.com/p05m048.

engage in analogous biological processes—such as cell wall construction and membrane dynamics—by interacting with different client proteins across bacterial species. Recent structural studies of SPFH proteins across domains of life reveal a remarkable ability to form cage-like architectures, albeit with varying cage sizes and membrane topologies[22,28]. These structural differences likely dictate protein localization, client interactions, and functional specialization. Collectively, our findings imply the evolutionary plasticity of SPFH proteins, where conserved structural principles are repurposed to meet the distinct physiological demands of prokaryotic and eukaryotic systems. This functional and mechanistic diversity not only highlights the adaptability of the SPFH protein family but also sets the stage for further exploration of their roles in cellular organization and dynamics.

Methods

Strains and growth conditions

Strains used in this study are listed in Supplementary Table 1. Solid MS (Mannitol Soy flour) medium[42] was used for collection of *Streptomyces* spores and for conjugation experiments, while MYM medium[43] was used for obtaining *Kitasatospora* spores. To compare colony sizes and observe the release of cell wall-deficient (CWD) cells under hyperosmotic stress, solid L-phase medium agar (LPMA) medium[8] or a modified LPMA medium (in which the 0.64 M sucrose was replaced with 0.32 M NaCl) were used. TSBS[42] medium was used to grow *Streptomyces* in liquid medium without hyperosmotic stress. For quantification of the number of CWD cells, as well as measurement of hyphal diameters and membrane fluidity, liquid L-phase broth (LPB) was used[8]. Briefly, 10^6 CFU ml^{-1} spores were inoculated in 20 ml LPB in 50 ml flasks without coil while shaking at 100 rpm ml^{-1}. All *Streptomyces* and *Kitasatospora* strains were grown at 30 °C. For hyphal branching detection, spores were inoculated onto cellophane membranes overlaying LPMA plates, which were then incubated at 30 °C for 16 h prior to analysis. Lysozyme sensitive assay were performed essentially as described[19]. Briefly, approximately 1000 spores of each strain were plated on Difco nutrient agar plates either or not supplemented with 0.25 mg ml^{-1} lysozyme (from chicken egg white, ≥40,000 units mg^{-1}, Sigma). After 48 h of growth, the total number of colonies was counted. For every strain, percentage of the number of colonies on the plate with lysozyme relative to the number of colonies on the plate without lysozyme as an estimate for lysozyme sensitivity.

E. coli DH5α[44] was used for cloning and β-lactamase experiments. *E. coli* BL21 (DE3)[45] and BTH101[46] were used in protein expression and bacterial two-hybrid assays, respectively. For conjugation, *E. coli* ET12567 harboring pUZ8002 was used. All *E. coli* strains were grown in LB medium at 37 °C with appropriate antibiotics, if needed.

Plasmid construction and transformation

Plasmids and primers used in this study are listed in Supplementary Tables 2 and 3, respectively.

To create the Δ*stlP*$_{FL}$ mutant (i.e., the *stlP* mutant in which the entire coding sequence of *stlP* was removed), the unstable multi-copy vector pWHM3-oriT was used as described[47]. The 1.2 kb of upstream and downstream regions of the *stlP* were amplified from genomic DNA of *S. coelicolor* with primer pairs LArm-F/LArm-R and RArm-F/RArm-R, respectively. The apramycin resistance cassette *aac(3) IV* flanked by *loxP* sites was amplified from plasmid pGWS728[48] using primers Apra-F/Apra-R. Amplified PCR products were Gibson assembled with XbaI-linearized pWHM3-oriT, yielding plasmid pXZ44.

For complementation of the *stlP* mutant, the coding sequence of *stlP* (SCO2834) was amplified from genomic DNA of *S. coelicolor* with primers stlP-F/stlP-R1. The PCR product was ligated as an NdeI/BamHI fragment into plasmid hpXZ2[19] harboring the constitutive *gapAp* prompter of SCO1947, yielding plasmid pXZ15.

For localization of StlP and DivIVA, the mCherry reporter was fused to the C-terminus of these two proteins. Coding sequences for *stlP* and *divIVA* were amplified from genomic DNA of *S. coelicolor* with primers stlP-F/stlP-R2 and 2077-F/2077-R, respectively. The gene encoding for mCherry was amplified from plasmid pGWS791[29] using primers mCh-F/mCh-R. After digestions with NdeI/HindIII (for *stlP* and *divIVA*) and HindIII/XbaI (for *mCherry*), combinations of *stlP/mCherry* and *divIVA/mCherry* were ligated with plasmid hpXZ2 that was cut with NdeI/XbaI, generating plasmid pXZ16 and pXZ17, respectively.

To constitutively express the HflK/C-like protein BOQ63_030050 in *Kitasatospora viridifaciens* and the *S. coelicolor stlP* mutant, the coding sequence of BOQ63_030050 was amplified from genomic DNA of *K. viridifaciens* DSM40239 with primers 0050-F/0050-R. The PCR product was ligated as an NdeI/XbaI fragment into plasmid hpXZ2 harboring the constitutive *gapAp* prompter, yielding plasmid pXZ41.

To express the stomatin-encoding domain of StlP (StlP$_{SD}$) in *E. coli*, nucleotides 610-1107 of *stlP* were amplified from *S. coelicolor* genomic DNA with primers 2834$_{sto}$-F/2834$_{sto}$-R and ligated into pET28a plasmid as a NdeI and HindIII fragment, yielding plasmid pXZ18. Consequently, StlP$_{SD}$ was expressed carrying a N-terminal Histidine-tag (6xHis).

For construction of the plasmids used in the pull-down assays, nucleotides 298-1152 of *stlP* were amplified with primers StlP-Fc/StlP-Rc and ligated into pACYCDuet-1 plasmid via NcoI and NdeI, yielding plasmid pXZ42. The coding sequence of *cslA* (SCO2836) and *glxA* (SCO2837) were amplified form *S. coelicolor* M145 genomic DNA with primer combinations CslA-F/CslA-R and GlxA-F/GlxA-R, respectively. The amplified fragments were sequentially ligated into pETDuet-1 using NcoI/HindIII (for inserting *cslA*) and NdeI/XhoI (for inserting *glxA*), yielding pXZ43. Using these plasmids, StlP and CslA are expressed with a C-terminal 8×Histidine-tag and Flag-tag, respectively, while GlxA was expressed without any tags.

To construct plasmids used in the biofluorescence complementation assay, enhanced GFP (eGFP) was split into two fragments as previously described[49]. the N-terminal fragment (eGFP$_N$), comprising amino acid residues 1–158, and the C-terminal portion (eGFP$_C$),

consisting of residues 159–239. The $eGFP_N$ and $eGFP_C$ fragments were then fused to either the N- or C-terminus of the target proteins (StlP, CslA and GlxA) via a flexible linker sequence, GSGGSG. To this end, combinations of PCR products were assembled using Gibson assembly into the pSET152 or pWHM3-oriT vector that have been digested with BamHI, which generates plasmids expressing various proteins fusions, under the control of constitutive *gapAp* promoter (see Supplementary Table 4 for details).

All plasmids were introduced into *E. coli* and *Streptomyces* via heat-shock transformation[50] and conjugation[42], respectively.

Inactivation of *stlP* in *Streptomyces*

For inactivation of *stlP* in *S. coelicolor*, we used cosmid StE20 carrying the Tn5062 transposon inserted after nucleotide position 892 relative to the start site of *stlP* (kindly provided by Prof. Paul Dyson, see Supplementary Table 2). This cosmid was introduced into *S. coelicolor* via conjugation using ET12567/pUZ8002[42], after which exconjugants were screened as described[51]. Colonies that were kanamycin-sensitive and apramycin-resistant were selected and used for further analysis. Mutants carrying the expected phenotype were verified by sequencing.

Growth curve generation

For preparing germinated spores, spores of different strains were resuspended in double-strength germination medium[42] at a final concentration of 10^6 CFU ml^{-1} and incubated at 30 °C for 6–8 h while shaking at 200 rpm min^{-1}. For generating the biomass growth curve, the RoboLector L-4-BL-II equipped with a parallelized shaken cultivation device was used[52]. Briefly, the germinated spores were centrifuged and resuspended in either TSBS or LPB media before being distributed (1 ml per well) into a 48-well FlowerPlates (Basesweiler Germany). The temperature and humidity were set at 30 °C and 85%, respectively. The biomass was collected automatically and measured in arbitrary units. All measurements were performed in triplicate.

Bacterial 2-hybrid analysis

To assess interactions of StlP with other tip-localizing proteins, the bacterial hybrid assay was used[46]. Therefore, *lpmP* (SCO2833), *stlP* (SCO2834), *sco2835*, *cslA* (SCO2836), *glxA* (SCO2837), *cslZ* (SCO2838), *divIVA* (SCO2077), *filP* (SCO5396) and *scy* (SCO5397) were amplified using primers Th2833-F/Th2833-R, Th2834-F/Th2834-R, Th2835-F/Th2835-R, Th2836-F/Th2836-R, Th2837-F/Th2837-R, Th2838-F/Th2838-R, divIVA-F/divIVA-R, filP-F/filP-R and scy-F/scy-R, respectively. All amplified DNA fragments were cloned into the pKT25 and pUT18C plasmids using EcoRI and XbaI, yielding plasmids pXZ19 (pUT18C + *lpmP*), pXZ20 (pKT25 + *stlP*), pXZ21 (pUT18C + *stlP*), pXZ22 (pKT25 + *SCO2835*), pXZ23 (pUT18C + *SCO2835*), pXZ24 (pKT25 + *cslA*), pXZ25 (pUT18C + *cslA*), pXZ26 (pKT25 + *glxA*), pXZ27 (pUT18C + *glxA*), pXZ28 (pKT25 + *cslZ*), pXZ29 (pKT25 + *divIVA*), pXZ30 (pUT18C + *divIVA*), pXZ31 (pKT25 + *filP*), pXZ32 (pUT18C + *filP*), pXZ33 (pKT25 + *scy*) and pXZ34 (pUT18C + *scy*) (see Supplementary Table 2).

E. coli BT101 carrying combinations of these constructs were used in bacterial 2-hybrid experiments to evaluate protein interactions as described[53].

Topology determination of StlP

To study the transmembrane topology of StlP, the β-lactamase-encoding gene *blaM* without its signal sequence was fused to the 3′ end of *stlP*, as described previously[29]. Only if BlaM is secreted, cells will be resistant to ampicillin. To this end, a *blaM* variant lacking the region encoding the signal sequence for secretion ($blaM_{NS}$) was amplified from plasmid pHJL401[54] with primers blaM-F/blaM-R. In parallel, full length *blaM* (including the region for the signal sequence, hereinafter referred to as $blaM_{FL}$) was amplified from the same plasmid using the $blaM_{FL}$-F/blaM-R primers. The *stlP* gene was amplified from *S. coelicolor* genomic DNA using primers stlP-F/*stlP*-R3. Subsequently, the amplified products were cut using restriction enzymes NdeI-HindIII (*stlP*), HindIII-EcoRI ($blaM_{NS}$) and NdeI-EcoRI ($blaM_{FL}$), and digested combinations of *stlP*/$blaM_{NS}$, and $blaM_{FL}$ were separately ligated into pXZ2[19] that was cut with NdeI-EcoRI, yielding pXZ35 and pXZ36 (see Supplementary Table 2).

E. coli DH5α harboring plasmid pSET152, pXZ35 and pXZ36 were used to assess the membrane topology of StlP, which were performed as described previously[29]. Full-length BlaM ($BlaM_{FL}$) expressed from pXZ36 served as a control for β-lactamase activity in the medium.

Quantification of CWD cells

Culturing and filtration of CWD cells of *Streptomyces* and *Kitasatospora* strains was essentially performed as described[8], with the exception that *S. coelicolor* strains were grown for 16 h, while *K. viridifaciens* strains were grown for 40 h. Quantification of CWD cells was performed with a Bright-Line™ Hemocytometer (Merck), as described[55]. Briefly, 10 µl of filtered culture supernatant were loaded into the counting chamber, after which cells were quantified under a Zeiss Axio microscope equipped with an Axiocam 105 camera. CWD cell numbers were counted manually, and the density was calculated. For each strain, the measurements were performed in triplicate.

Protein expression and purification

To purify the stomatin-encoding domain of StlP ($StlP_{SD}$), *E. coli* BL21 (DE3) cells harboring plasmid pXZ17 were cultured at 37 °C to an OD_{600} of 0.8 in LB medium containing 50 mg ml^{-1} kanamycin. Then, 0.5 mM isopropyl β-D-thiogalactopyranoside was added to induce protein expression, after which cells were grown at 30 °C for 18 h. The induced cells were subsequently lysed by sonication in binding buffer (50 mM Tris–HCl, 200 mM NaCl, pH 8.0), and after centrifugation, the lysate was loaded on a Ni^{2+}-chelating column equilibrated with binding buffer. Ten column volumes of washing buffer (50 mM Tris–HCl, 200 mM NaCl, 0.1 mM imidazole, pH 8.0) and 5 mL of elution buffer (50 mM Tris–HCl, 200 mM NaCl, 10 mM imidazole, pH 8.0) were used to wash and elute $StlP_{SD}$, respectively. Finally, the protein was purified by gel filtration using a Hiload 16/600 Superdex 200 pg column (GE Healthcare) equilibrated with buffer (50 mM Tris–HCl, 100 mM NaCl, pH 8.0). Sample fractions were analyzed on a 12.5% SDS-PAGE gel. Fractions were stored directly at −80 °C or first concentrated to 1 mg ml^{-1} with the 3 kDa molecular weight cutoff concentrator (Millipore) and then stored.

Pull-down experiments

The pull-down assay of StlP-8His with CslA-Flag and GlxA was performed with heterologous *E. coli* BL21 (DE3) cells harboring plasmid pXZ42 and pXZ43. Cells were cultured at 37 °C in Terrific Broth (TB) medium containing 50 mg ml^{-1} ampicillin and 25 mg ml^{-1} chloramphenicol. The subsequent protein purification was largely performed as previously described[17], with some modifications. Briefly, the induced cells were collected and then lysed by sonication. Subsequently, the crude membranes were collected and solubilized. After removing the insoluble membrane fraction by centrifugation, the soluble membrane fraction was incubated overnight at 4 °C with equilibrated Ni^{2+} resin. The resin was packed in a gravity flow chromatography column and washed with 50 mL modified WB1 buffer containing 50 mM phosphate buffer, pH 7.2, 200 mM NaCl, 8% glycerol, 60 mM imidazole and 0.02% DDM (n-Dodecyl-β-D-Maltoside, Sigma). Proteins were eluted with 15 mL elution buffer containing 50 mM phosphate buffer, pH 7.2, 200 mM NaCl, 8% glycerol, 500 mM imidazole and 0.02% DDM.

For SEC analysis, the eluted protein complexes were concentrated using 100-kDa cut-off Amicon® ultra centrifugal filters (Millipore) before being loaded into the Superdex 200 Increase 10/300 GL column, which has been equilibrated with buffer

containing 50 mM phosphate buffer, pH 7.2, 200 mM NaCl, 8% glycerol and 0.02% DDM.

SDS-/Native-PAGE and immunoblotting assay

SDS- and Native-PAGE analyses were performed using the Bio-Rad Mini-PROTEIN system with manually-made 7.5% gels and 12% Mini-PROTEAN® TGX™ Precast Protein Gels (BIO-RAD), respectively. Coomassie Brilliant Blue (Sigma) was used to visualize protein bands. The proteins were detected by immunoblotting, which was essentially performed as described[18]. For the detection of the StlP-8×His, CslA-Flag and β-lactamase, the His-tag and DYKDDDDK tag monoclonal antibodies (Proteintech) and β-lactamase monoclonal antibody (Thermo Fisher) were used as the primary antibodies, respectively. Subsequently, anti-Mouse IgG-Alkaline Phosphatase (Sigma) was used as the secondary antibody. The primary and secondary antibodies used for detection of GlxA were identical to those described[18]. Images were collected using an Epson Perfection V37 scanner.

Microscopy

To visualize the emergence of CWD cells, spores of the wild-type strain and the Δ*stlP* mutant were pre-germinated in double strength germination medium[42]. Then 10 µl of germlings were used for live-imaging, for which an ibiTreat 35 mm low imaging dish (ibidi) and a LPMA-pad was used as before[8]. Live imaging was carried out using a Zeiss LSM900 Airyscan 2 microscope. If necessary, Z-Stack acquisitions were used. For visualization of membrane and nucleic acids, 0.05 mg ml^{-1} FM5-95 and 0.5 µM SYTO-9 (Sigma) were used, respectively.

The detection of nascent peptidoglycan was done by using BODIPY-FL vancomycin (Sigma), essentially as described[56]. Briefly, after growing *Streptomyces* strains in LPB medium for 16 h, mycelia were collected (3300 × *g*, 10 min) and resuspended in 200 µl of fresh LPB medium containing 1 µg ml^{-1} BODIPY-FL vancomycin and 1 µg ml^{-1} vancomycin. After 10 min incubation at 30 °C, the mycelia were washed 3 times with PBS. Five µl of the washed mycelia was used for microscopy analysis using a Zeiss LSM900 Airyscan 2 microscope.

For visualizing fluid membrane microdomains, mycelia were stained with $DilC_{12}$[31,32]. Briefly, $DilC_{12}$ was dissolved in DMSO and 10 mg ml^{-1} stock was prepared. For sample preparation, spores of each strain were inoculated in LPB medium at a final concentration of 10^6 CFU ml^{-1}. After 16 h of growth, mycelia were collected by centrifuge (3300 × *g*, 10 min) and resuspended in prewarmed fresh LPB medium supplemented with 100 µg ml^{-1} $DilC_{12}$, followed by growth for 3 h at 30 °C while shaking at 100 rpm min^{-1}. Then, mycelia were collected, washed 3 times with prewarmed LPB supplemented with 1% DMSO, and resuspended in the same wash buffer. $DilC_{12}$ signal was detected via a Cy3 filter (535 nm excitation and 590 nm emission) using a Zeiss LSM900 Airyscan 2 microscope, wherein the cultivation chamber had been set 30 °C to avoid temperature changes during imaging.

For measurement of membrane fluidity, samples were prepared essentially as described[26]. Briefly, Laurdan (6-Dodecanoyl-N, N-dymethyl2-naphthylamine, Sigma) was dissolved in dimethylformamide (DMF) and a 10 mM stock was prepared. For preparation of mycelia for Laurdan staining, 20 ml 16 h-old mycelia were collected (3300 × *g*, 10 min) and resuspended in 1 ml 30 °C pre-warmed LPB medium containing 1 mM Laurdan. For sample preparation of the *stlP* mutant, the culture was filtrated through a 100 µm cut-off filter (Falcon Cell Strainer 100 µm Nylon) to remove the majority of the CWD cells. The filtered mycelium was resuspended in 1 ml 30 °C pre-warmed LPB medium and used for Laurdan staining. After 10 min incubation in the dark at 30 °C, stained mycelia were collected again and washed twice in 30 °C pre-warmed PBS buffer supplemented with 20% sucrose and 1% DMF and finally resuspended in 200 µl pre-warmed PBS buffer supplemented with 20% sucrose. Fluorescent intensities were measured at 435 and 490 nm, following excitation at 350 nm using a Zeiss LSM900 Airyscan 2 microscope, wherein the cultivation chamber had been set 30 °C to avoid temperature changes during imaging. To calculate the membrane fluidity at hyphal tips, the tip region was cropped as a square (1 µm × 1 µm) from the image and the corresponding generalized polarization (GP) value was determined using ImageJ software in combination with the macro tool CalculateGP designed by Norbert Vischer (https://sils.fnwi.uva.nl/bcb/objectj/examples/CalculateGP/MD/gp.html) as described[57].

For measurement of hyphal diameters, 16 h-old mycelia were collected (3300 × *g*, 10 min) and resuspended in fresh LPB medium containing 0.05 mg ml^{-1} FM5-95. The distance between the stained membranes was used to measure the hyphal diameters by averaging the diameter at 3 distinct spots in the hypha.

The cellulose-like glycan at hyphal tips was visualized by calcofluor white (Sigma) staining and quantified as previous described[19]. Briefly, 10^6 CFU ml^{-1} spores were inoculated in 20 ml LPB in 50 ml flasks without coil while shaking at 100 rpm ml^{-1}. After 16 h of growth, mycelia were collected (3300 × *g*, 10 min) and resuspended in 200 µl fresh LPB medium containing 100 µg ml^{-1} Calcofluor white (Thermo Fisher, catalog R21507). After staining for 10 min at room temperature, 5 µl of the stained mycelia was used for microscopy analysis using a Zeiss LSM900 Airyscan 2 microscope. For quantitatively comparing fluorescence, the measure region with the size of 15 µm × 15 µm squares at hyphal tips was used.

For analysis of hyphal branching patterns, mycelium was grown from single spore and imaged using a Zeiss Axio microscope equipped with an Axiocam 105 camera as described previously[19]. The distance from the tip to the proximal branch point was measured. A proximal branch was defined as having a length of 1–4 µm as previous described[58].

For measurement of colony sizes, strain were grown on LPMA medium in petri dishes with a 9 cm diameter aiming for ±100 colonies per plate. After growing them for 5–7 days at 30 °C, plates were scanned with Epson Perfection V37 scanner and colony size was measured subsequently.

For biofluorescence complementation assay, spores of each strain (M145 + pXZ45, M145 + pXZ46, M145 + pXZ47, M145 + pXZ48, M145 + pXZ49, M145 + pXZ50, M145 + pXZ51, M145 + pXZ45 + pXZ47, M145 + pXZ45 + pXZ48, M145 + pXZ46 + pXZ47, M145 + pXZ46 + pXZ48, M145 + pXZ45 + pXZ49, M145 + pXZ46 + pXZ49, M145 + pXZ50 + pXZ49, M145 + pXZ51 + pXZ49) were inoculated in LPB medium at a final concentration of 10^6 CFU ml^{-1}. After 16–24 h of growth (depends on the growth speed), mycelia were collected by centrifuge (3300 × *g*, 10 min) and signal of eGFP at hyphal tips were detected using the Zeiss LSM900 Airyscan 2 microscope. All measurement and images processing were executed with ImageJ software (version 2.0.0/1.53c/Java 1.8.0_172/64-bit).

Sacculus isolation and cryo-electron tomography

Isolation of sacculi of *S. coelicolor* M145 and the *stlP* mutant was essentially performed as described[59], except that 16 h-old liquid cultures were used and the step of removing teichoic acids was neglected.

Sample preparation for cryo-electron tomography (cryo-ET) was performed as described[59]. Briefly, after adding the colloidal gold beads, sacculi solutions were vitrificated and applied on the EM grids. Grids were examined using a 120 kV Talos TEM (FEI/Thermo Fisher) and cryo-ET data were collected using a Titan Krios instrument (Thermo Fisher Scientific). The measurement of cell wall thickness was performed as described[59].

Bioinformatic analysis

Protein domains and protein structures were predicted by InterPro (https://www.ebi.ac.uk/interpro/) and AlphaFold 2.0[60]. The prediction of protein membrane topology was performed by TransMembrane Hidden Markov Model (TMHMM) (Version 2.0) (https://services.

healthtech.dtu.dk/service.php?TMHMM-2.0). Alignment of protein structures was done by PyMOL software (Version 2.5). Amino acids sequence alignment was done by ESPript 3.0 (https://espript.ibcp.fr/ESPript/cgi-bin/ESPript.cgi).

To phylogenetically compare StlP with other SPFH proteins, MEGA 7 was used. Amino acid sequences of all SPFH proteins were downloaded from the UniProt database. For phylogenetic analysis of the distribution of StlP, the amino acid sequence of StlP was used to run Position-Specific Iterative (PSI)-BLAST to find homologs in the dataset of 15405 reference sequence database (RefSeq) representative bacteria and archaea. The homologs with a bitscore >130 were chosen and subsequently each hit was subjected to membrane topology prediction using TMHMM server (Version 2.0). Only hits with an identical membrane topology were considered valid StlP homologs. The phylogenetic tree was annotated using iTOL (https://itol.embl.de/).

Statistical analyses and reproducibility

For statistical analyses, GraphPad Prism software (version 8.0.2) was used. $p < 0.05$ was considered as significance. All experiments were repeated at least three times with similar results.

Reporting summary

Further information on research design is available in the Nature Portfolio Reporting Summary linked to this article.

Data availability

The predicted protein structures have been deposited in Figshare (https://figshare.com/articles/media/Predicted_StlP_structures/26161969). Source data are provided with this paper.

References

1. Cabeen, M. T. & Jacobs-Wagner, C. Bacterial cell shape. *Nat. Rev. Microbiol.* **3**, 601–610 (2005).
2. Mueller, E. A. & Levin, P. A. Bacterial cell wall quality control during environmental stress. *mBio* **11**, e02456–02420 (2020).
3. Daniel, R. A. & Errington, J. Control of cell morphogenesis in bacteria: two distinct ways to make a rod-shaped cell. *Cell* **113**, 767–776 (2003).
4. Letek, M. et al. DivIVA is required for polar growth in the MreB-lacking rod-shaped actinomycete *Corynebacterium glutamicum*. *J. Bacteriol.* **190**, 3283–3292 (2008).
5. Flärdh, K. Growth polarity and cell division in *Streptomyces*. *Curr. Opin. Microbiol.* **6**, 564–571 (2003).
6. Flärdh, K. Cell polarity and the control of apical growth in *Streptomyces*. *Curr. Opin. Microbiol.* **13**, 758–765 (2010).
7. Brown, A. D. Microbial water stress. *Bacteriol. Rev.* **40**, 803–846 (1976).
8. Ramijan, K. et al. Stress-induced formation of cell wall-deficient cells in filamentous actinomycetes. *Nat. Commun.* **9**, 5164 (2018).
9. Flärdh, K. Essential role of DivIVA in polar growth and morphogenesis in *Streptomyces coelicolor* A3(2). *Mol. Microbiol.* **49**, 1523–1536 (2003).
10. Fröjd, M. J. & Flärdh, K. Apical assemblies of intermediate filament-like protein FilP are highly dynamic and affect polar growth determinant DivIVA in *Streptomyces venezuelae*. *Mol. Microbiol.* **112**, 47–61 (2019).
11. Holmes, N. A. et al. Coiled-coil protein Scy is a key component of a multiprotein assembly controlling polarized growth in *Streptomyces*. *Proc. Natl Acad. Sci. USA* **110**, E397–E406 (2013).
12. Mukherjee, P. et al. Novel role of Wag31 in protection of mycobacteria under oxidative stress. *Mol. Microbiol.* **73**, 103–119 (2009).
13. Meniche, X. et al. Subpolar addition of new cell wall is directed by DivIVA in mycobacteria. *Proc. Natl Acad. Sci. USA* **111**, E3243–E3251 (2014).
14. Walshaw, J., Gillespie, M. D. & Kelemen, G. H. A novel coiled-coil repeat variant in a class of bacterial cytoskeletal proteins. *J. Struct. Biol.* **170**, 202–215 (2010).
15. Ditkowski, B. et al. Dynamic interplay of ParA with the polarity protein, Scy, coordinates the growth with chromosome segregation in *Streptomyces coelicolor*. *Open Biol.* **3**, 130006 (2013).
16. Xu, H., Chater, K. F., Deng, Z. & Tao, M. A cellulose synthase-like protein involved in hyphal tip growth and morphological differentiation in *Streptomyces*. *J. Bacteriol.* **190**, 4971–4978 (2008).
17. Zhong, X. et al. CslA and GlxA from *Streptomyces lividans* form a functional cellulose synthase complex. *Appl. Environ. Microbiol.* **90**, e0208723 (2024).
18. Chaplin, A. K. et al. GlxA is a new structural member of the radical copper oxidase family and is required for glycan deposition at hyphal tips and morphogenesis of *Streptomyces lividans*. *Biochem. J.* **469**, 433–444 (2015).
19. Zhong, X., Zhang, L., van Wezel, G. P., Vijgenboom, E. & Claessen, D. Role for a lytic polysaccharide monooxygenase in cell wall remodelling. *mBio* **13**, e00456–00422 (2022).
20. Browman, D. T., Hoegg, M. B. & Robbins, S. M. The SPFH domain-containing proteins: more than lipid raft markers. *Trends Cell Biol.* **17**, 394–402 (2007).
21. Langhorst, M. F., Reuter, A. & Stuermer, C. A. O. Scaffolding microdomains and beyond: the function of reggie/flotillin proteins. *Cell. Mol. Life Sci.* **62**, 2228–2240 (2005).
22. Fu, Z. & MacKinnon, R. Structure of the flotillin complex in a native membrane environment. *Proc. Natl Acad. Sci. USA* **121**, e2409334121 (2024).
23. López, D. & Kolter, R. Functional microdomains in bacterial membranes. *Genes Dev.* **24**, 1893–1902 (2010).
24. Zielińska, A. et al. Flotillin-mediated membrane fluidity controls peptidoglycan synthesis and MreB movement. *eLife* **9**, e57179 (2020).
25. García-Fernández, E. et al. Membrane microdomain disassembly inhibits MRSA antibiotic resistance. *Cell* **171**, 1354–1367 (2017).
26. Bach, J. N. & Bramkamp, M. Flotillins functionally organize the bacterial membrane. *Mol. Microbiol.* **88**, 1205–1217 (2013).
27. Huang, X., Gaballa, A., Cao, M. & Helmann, J. D. Identification of target promoters for the *Bacillus subtilis* extracytoplasmic function σ factor, σ W. *Mol. Microbiol.* **31**, 361–371 (1999).
28. Ma, C. et al. Structural insights into the membrane microdomain organization by SPFH family proteins. *Cell Res.* **32**, 176–189 (2022).
29. Zhang, L., Willemse, J., Claessen, D. & van Wezel, G. P. SepG coordinates sporulation-specific cell division and nucleoid organization in *Streptomyces coelicolor*. *Open Biol.* **6**, 150164 (2016).
30. Lapatsina, L., Brand, J., Poole, K., Daumke, O. & Lewin, G. R. Stomatin-domain proteins. *Eur. J. Cell Biol.* **91**, 240–245 (2012).
31. Strahl, H., Bürmann, F. & Hamoen, L. W. The actin homologue MreB organizes the bacterial cell membrane. *Nat. Commun.* **5**, 3442 (2014).
32. Wenzel, M., Vischer, N. O. E., Strahl, H. & Hamoen, L. W. Assessing membrane fluidity and visualizing fluid membrane domains in bacteria using fluorescent membrane dyes. *Bio Protoc.* **8**, e3063–e3063 (2018).
33. Müller, A. et al. Daptomycin inhibits cell envelope synthesis by interfering with fluid membrane microdomains. *Proc. Natl Acad. Sci. USA* **113**, E7077–E7086 (2016).
34. Bramkamp, M. & Scheffers, D. J. Bacterial membrane dynamics: compartmentalization and repair. *Mol. Microbiol.* **120**, 490–501 (2023).
35. Ultee, E., Zhong, X., Shitut, S., Briegel, A. & Claessen, D. Formation of wall-less cells in *Kitasatospora viridifaciens* requires cytoskeletal protein FilP in oxygen-limiting conditions. *Mol. Microbiol.* **115**, 1181–1190 (2021).

36. Wetzel, C. et al. A stomatin-domain protein essential for touch sensation in the mouse. *Nature* **445**, 206–209 (2007).
37. Brand, J. et al. A stomatin dimer modulates the activity of acid-sensing ion channels. *EMBO J.* **31**, 3635–3646 (2012).
38. Takekawa, N. et al. Structure of *Vibrio* FliL, a new stomatin-like protein that assists the bacterial flagellar motor function. *mBio* **10**, e00292–00219 (2019).
39. Yokoyama, H., Fujii, S. & Matsui, I. Crystal structure of a core domain of stomatin from *Pyrococcus horikoshii* illustrates a novel trimeric and coiled-coil fold. *J. Mol. Biol.* **376**, 868–878 (2008).
40. Dannenberg, N. et al. Mycobacteria form viable cell wall-deficient cells that are undetectable by conventional diagnostics. *bioRxiv* https://doi.org/10.1101/2022.11.16.516772 (2022).
41. Takeshita, N., Diallinas, G. & Fischer, R. The role of flotillin FloA and stomatin StoA in the maintenance of apical sterol-rich membrane domains and polarity in the filamentous fungus *Aspergillus nidulans*. *Mol. Microbiol.* **83**, 1136–1152 (2012).
42. Kieser, T., Bibb, M. J., Buttner, M. J., Chater, K. F. & Hopwood, D. A. *Practical Streptomyces Genetics* (The John Innes Foundation, 2000).
43. Stuttard, C. Temperate phages of *Streptomyces venezuelae*: lysogeny and host specificity shown by phages SV1 and SV2. *J. Gen. Microbiol.* **128**, 115–121 (1982).
44. Taylor, R. G., Walker, D. C. & McInnes, R. R. *E. coli* host strains significantly affect the quality of small scale plasmid DNA preparations used for sequencing. *Nucleic Acids Res.* **21**, 1677–1678 (1993).
45. Kim, S. et al. Genomic and transcriptomic landscape of *Escherichia coli* BL21 (DE3). *Nucleic Acids Res.* **45**, 5285–5293 (2017).
46. Karimova, G., Pidoux, J., Ullmann, A. & Ladant, D. A bacterial two-hybrid system based on a reconstituted signal transduction pathway. *Proc. Natl Acad. Sci. USA* **95**, 5752–5756 (1998).
47. Wu, C. et al. Lugdunomycin, an angucycline-derived molecule with unprecedented chemical architecture. *Angew. Chem.* **58**, 2809–2814 (2019).
48. Zhang, L., Willemse, J., Hoskisson, P. A. & van Wezel, G. P. Sporulation-specific cell division defects in *ylmE* mutants of *Streptomyces coelicolor* are rescued by additional deletion of *ylmD*. *Sci. Rep.* **8**, 7328 (2018).
49. Ghosh, I., Hamilton, A. D. & Regan, L. Antiparallel leucine zipper-directed protein reassembly: application to the green fluorescent protein. *J. Am. Chem. Soc.* **122**, 5658–5659 (2000).
50. Hanahan, D. Studies on transformation of *Escherichia coli* with plasmids. *J. Mol. Biol.* **166**, 557–580 (1983).
51. Fernández-Martínez, L. T. et al. A transposon insertion single-gene knockout library and new ordered cosmid library for the model organism *Streptomyces* coelicolor A3 (2). *Antonie Van Leeuwenhoek* **99**, 515–522 (2011).
52. Koepff, J. et al. Fast and reliable strain characterization of *Streptomyces lividans* through micro-scale cultivation. *Biotechnol. Bioeng.* **114**, 2011–2022 (2017).
53. Krasteva, P. V. et al. Insights into the structure and assembly of a bacterial cellulose secretion system. *Nat. Commun.* **8**, 2065 (2017).
54. Larson, J. L. & Hershberger, C. L. The minimal replicon of a streptomycete plasmid produces an ultrahigh level of plasmid DNA. *Plasmid* **15**, 199–209 (1986).
55. Paul Jr, F. *Tissue Culture: Methods and Applications* (Elsevier, 2012).
56. van der Aart, L. T., Lemmens, N., van Wamel, W. J. & van Wezel, G. P. Substrate inhibition of VanA by d-alanine reduces vancomycin resistance in a VanX-dependent manner. *Antimicrob. Agents Chemother.* **60**, 4930–4939 (2016).
57. Kapteijn, R. et al. Endocytosis-like DNA uptake by cell wall-deficient bacteria. *Nat. Commun.* **13**, 5524 (2022).
58. Passot, F. M., Cantlay, S. & Flärdh, K. Protein phosphatase SppA regulates apical growth and dephosphorylates cell polarity determinant DivIVA in *Streptomyces coelicolor*. *Mol. Microbiol.* **117**, 411–428 (2022).
59. Ultee, E. et al. Teichoic acids anchor distinct cell wall lamellae in an apically growing bacterium. *Commun. Biol.* **3**, 314 (2020).
60. Mirdita, M. et al. ColabFold: making protein folding accessible to all. *Nat. Methods* **19**, 679–682 (2022).

Acknowledgements

This work was funded by a Vici grant (VI.C.192.002) from the Dutch Research Council to Dennis Claessen and a grant from the Deutsche Forschungsgemeinschaft (BR2815/7-1) to S.S.M.B.

Author contributions

X.Z. conducted the majority of the experiments. S.M.B. and S.S. assisted with the membrane fluidity analysis. V.O. carried out the sacculi imaging using Cryo-ET. G.G.E. and C.D. performed the phylogenetic analyses. E.V., G.P.W., V.C.B., A.B., and M.B. provided guidance and manuscript editing. D.C. oversaw the project. X.Z. and D.C. prepared the manuscript.

Competing interests

The authors declare no competing interests.

Additional information

Supplementary information The online version contains supplementary material available at https://doi.org/10.1038/s41467-025-58093-x.

Correspondence and requests for materials should be addressed to Dennis Claessen.

Peer review information *Nature Communications* thanks the anonymous reviewers for their contribution to the peer review of this work. A peer review file is available.